Structural and Multidisciplinary Optimization
https://doi.org/10.1007/s00158-021-02991-3

RESEARCH PAPER

Exploring various options for improving crashworthiness performance of rail vehicle crash absorbers with diaphragms

Sabri Alper Keskin[1] · Erdem Acar[1] · M. A. Güler[2] · Murat Altin[3]

Received: 15 March 2021 / Revised: 14 May 2021 / Accepted: 16 June 2021

Abstract

In this paper, the effects of various design options for improving the crashworthiness performance of a rectangular crash absorber with diaphragms are explored. These design options include (i) optimal tube and diaphragm dimensioning, (ii) optimal diaphragm placement, and (iii) tapering of the crash absorber. The wall thicknesses of the absorber and the diaphragms, the locations of the diaphragms, and the taper angle are taken as design variables to optimize the crashworthiness performance of the absorber. Before the optimization study, a finite element model is generated and validated with experimental results available in the literature. The effect of each design variable on crashworthiness performance is evaluated by solving a series of design optimization problems, and compared with the baseline design. A successive iterative approach is used in this study, where the optimum design variables obtained from a previous optimization problem are used as the initial design of the next optimization problem. Maximum specific energy absorption (SEA) is sought in these optimization problems. A surrogate-based optimization approach is used, where radial basis functions and response surface models are utilized. Optimal tube and diaphragm dimensioning resulted in 59.2% increase, optimum diaphragm placement led to 7.7% additional increase, and tapering resulted in 2.5% further increase in SEA. Overall, the design changes considered in this paper provided 69.4% increase in SEA.

Keywords Crash absorber · Diaphragms · Rail vehicle · Specific energy absorption · Surrogate-based optimization

1 Introduction

Crash absorbers are structures typically located in the front and rear ends of trains and cars. These structures are used for a controlled plastic deformation to absorb the crash energy and thereby contribute to the safety of passengers and vehicles. Various studies have been carried out to enhance the absorbers ability to withstand crashes while reducing the weight of these structures. For a detailed review of the recent developments in technology and design strategies for crash absorbers in passenger rail vehicles, the reader is referred to Gao and Wang (2019).

Thin-walled tubes are widely used as crash absorbers in train and automobiles as they are inexpensive and efficient in terms of energy absorption. The single-cell design can be considered the simplest form of a thin-walled tube as a crash absorber. In previous studies on single-cell crash absorbers, Mamalis et al. (2001) studied the effects of different taper angles on the crash absorption capability of rectangular cross-sectional crash absorbers with the same taper angle on every surface, while Nagel and Thambiratnam (2004) studied the crashworthiness effects of different taper angles in axisymmetric crash absorbers. Tarlochan et al. (2013) investigated the effect of the cross-sectional shape on axial and oblique crash problems, comparing circular, square, rectangular, hexagonal, octagonal and ellipse cross sections. Zhang and Zhang (2016) investigated the effects of different wall thicknesses in axisymmetric square crash absorbers. Abolfathi and Alavi Nia (2018) optimized radius, structure thickness and height, friction coefficient, contact area and impact angle with the mold-shaped impact surface in circular cross-sectional shock absorbers. Ming et al. (2019)

Responsible Editor: Nestor V Queipo

Special Issue dedicated to Dr. Raphael T. Haftka

✉ Erdem Acar
acar@etu.edu.tr

[1] Department of Mechanical Engineering, TOBB University of Economics and Technology, 06560, Ankara, Turkey

[2] College of Engineering and Technology, American University of the Middle East, Egaila, Kuwait

[3] Department of Automotive Engineering, Gazi University, Ankara, 06590, Turkey

Published online: 14 July 2021

studied the usage of kirigami pattern on design of single-cell crash absorbers, investigating the effects of kirigami shape parameters on crashworthiness.

Instead of using a single-cell design, vertical supports can be introduced to the structure to obtain a multi-cell design. Qi et al. (2012) studied the effects of different crash angles, comparing the crashworthiness of single and multi-cell crash absorbers. Song et al. (2013) optimized wall thickness, taper angle and foam density in single-cell crash absorbers supported with foam. An et al. (2015) optimized the wall thickness of a crash absorbers with square cross section and aluminum foam support. Wu et al. (2016) investigated the effects of different shape and form configurations of multi-cell crash structures on crashworthiness, and optimized thickness of walls, size of corner cells and location of connecting flanges in five-cell crash absorbers. Xiang et al. (2017) developed multi-cell crash absorbers containing a circular structure inside, once again taking inspiration from the internal structure of the beetle elytra, and investigated the impact of these designs on crashworthiness. Xiang and Du (2017) developed new forms of honeycomb structures, taking inspiration from the internal structure of the beetle elytra and studied the impact of these designs on crashworthiness. Xie et al. (2017) optimized cell amount, thickness of outer walls and length of outer sides for crashworthiness. Zhou et al. (2017) examined the effects of the form of the outer structure and the scale of the honeycomb cells on crashworthiness in crash absorbers supported with a honeycomb shaped inner structure. Zou et al. (2017a) explored the impact of different cross sections on axial and oblique crash absorbing capability, and thickness of the outer wall, thickness of the vertical support wall and length of the vertical support wall were optimized under different angles of impact. Altin et al. (2018) optimized the wall thickness, number of tubes, taper angle, aluminum foam density and the amount of aluminum foam placed into the structure in multi-cell crash absorbers. Wang et al. (2018) studied the effects of adding a concave crash absorber as a vertical support structure inspired by the human bone structures. Wang et al. (2019) and (Xu et al. 2019b) constructed hierarchical structures on vertical supports and investigated the effects of these structures on crashworthiness. Altin et al. (2019) studied the effects of vertically positioned support surfaces and the different cross sections created by these surfaces on crashworthiness.

The use of a multi-tubular design as opposed a single-tube design was found to improve the crashworthiness performance of thin-walled tubes. Zou et al. (2017b) optimized the effects of wall thickness for inner and outer tubes and the thickness of ribs connecting these two tubes. Deng and Liu (2019) used a three-tubular structure with a laterally corrugated middle tube, and investigated the effects of amplitude and number of corrugations alongside with the thickness of the corrugated tube.

Introducing cutouts and indentations was found to be a successful way of improving crash performance of thin-walled tubes. Acar et al. (2011) optimized cylindrical tapered tubes with lateral indentations to determine the optimum values of the number of the axisymmetric indentations, radius of the indentations, taper angle and wall thickness. Song and Guo (2013) compared the crashworthiness of multi-cell and windowed tubes on axial and oblique impacts. Song (2013) studied the effect of rectangular hole size on crash absorbers with square cross sections. Auersvaldt and Alves (2015) studied the effects of different sized rectangular windows on rectangular crash absorbers, comparing the absorbing metrics of different window sizes. Taştan et al. (2016) optimized wall thickness, taper angle, the cutout diameter and numbers of cutouts in horizontal and vertical directions in crash absorbers with circular cross sections. Nikkhah et al. (2017) studied the effects of different hole shapes on crash absorbers with square cross sections, investigating several crash evaluation metrics. Asanjarani et al. (2017) optimized the indentation cross section, taper angle, wall thickness, number of indentations and radius of indentations on tapered absorbers with rectangular cross sections. A dynamic crash problem was utilized in that study and the crash evaluation metrics were compared for each model under different crash velocities and angles. Nikkhah et al. (2019) found the optimum solutions for different crash absorber cross sections and hole shapes.

Another way to improve the crash performance of thin-walled tubes is to place diaphragms inside the crash absorbers. Gao et al. (2014) examined thickness of outer wall in crash absorbers with diaphragms on the energy absorption potential of vertical and angled impacts. Dong et al. (2015) investigated the effect of number of diaphragms, inner tube shape and inner tube size on bi-tubular structures for crashworthiness. Peng et al. (2015) examined the effects created by the change of wall thickness and material parameters of honeycomb structure on crash absorbers with square thin-walled crash absorbers containing guide rails and honeycomb structures mounted between diaphragms. Yao et al. (2018) investigated the effect of a modified honeycomb cross section for crash absorbing capabilities under crashes with horizontal and vertical offsets. Xu et al. (2019a) optimized thicknesses of all the diaphragms and outer tubes in axisymmetric rectangular crash absorbers with rectangle cross section. Xu et al. (2020) conducted the crashworthiness sensitivity analysis and pareto front optimization for diaphragm and outer tube thicknesses in a crash absorber with rectangular cross section and diaphragms.

In the existing studies on crash absorbers with diaphragms, the thicknesses of all diaphragms as well as the spacings between them are taken to be the same. The main contribution of this study to the existing literature is that the diaphragm thicknesses and the spacings between the diaphragms are allowed to take different values. Also, the effect of taper angle on the crashworthiness performance of a rectangular crash absorber with diaphragms is explored.

Since computational cost of crash simulations are expensive, surrogate-based approaches are widely used in crashworthiness optimization of crash absorbers and other thin-walled structures (Acar et al. 2011; Qi et al. 2012; Song et al. 2013; An et al. 2015; Taştan et al. 2016; Asanjarani et al. 2017; Fang et al. 2017; Xie et al. 2017; Abolfathi and Alavi Nia 2018; Altin et al. 2018; Wang et al. 2018; Nikkhah et al. 2019; Tyan and Lee 2019; Xu et al. 2019a) . Surrogate-based optimization is one of the fields where Prof. Raphael (Rafi) T. Haftka has made seminal contributions (Roux et al. (1998), Queipo et al. (2005), Goel et al. (2007), among others). This paper is dedicated to his memory.

The remainder of the paper is organized as follows. Design optimization of a rectangular tube with diaphragms against crash is discussed in Section 2. Finite element modeling is discussed in Section 3, and the validation of the finite element model is provided in Section 4. The effects of various design options are discussed in Section 5, followed by concluding remarks given in Section 6. To provide a better readability of the paper, details on surrogate-based optimization technique, surrogate models, error metrics, details of the different optimization problems are given in appendices.

2 Design optimization of rectangular tubes with diaphragms

Xu et al. (2019a) investigated crashworthiness design optimization of a rectangular tube with diaphragms by considering specific energy absorption (SEA) and initial peak crush force (IPCF). In their study, they considered three design variables: (i) wall thickness (A) of the long edge of the tube, (ii) wall thickness (B) of the short edge of the tube, (iii) the thickness (C) of the diaphragms (see Fig. 1).

Xu et al. (2019a) considered a multi-objective optimization study, while in this paper we focus our attention on optimization for maximum SEA to simplify the problem, because the additional design options that we include (i.e., optimal diaphragm placement, and tapering of the crash absorber) have larger impact on SEA than IPCF. Design optimization for maximum SEA with a limit on EA can be formulated as:

$$\begin{aligned} \text{Find} \quad & A, B, C_u \\ \text{Max} \quad & \text{SEA}(A, B, C_u) \\ \text{s.t.} \quad & \text{EA}(A, B, C_u) \geq 70 \text{ kJ} \\ & 2 \text{ mm} \leq A \leq 6 \text{ mm} \\ & 2 \text{ mm} \leq B \leq 6 \text{ mm} \\ & 2 \text{ mm} \leq C_u \leq 6 \text{ mm} \end{aligned} \tag{1}$$

As seen from (1), the crashworthiness characteristics of the crash absorbers are evaluated using two metrics: EA and SEA. Total energy absorbed (EA) refers to the amount of energy dissipated by the crash absorber. It can be measured

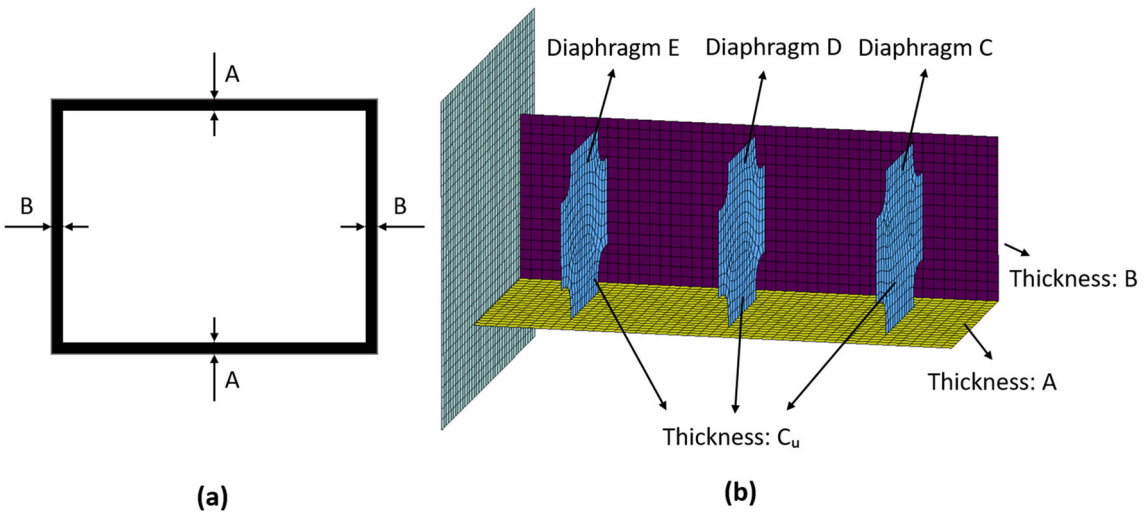

Fig. 1 Design variables used in Xu et al. (2019a)

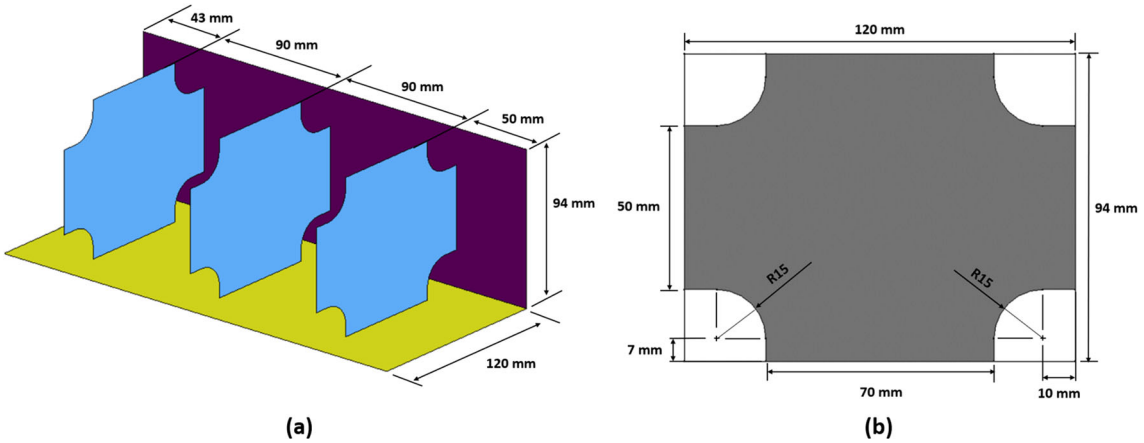

Fig. 2 Dimensions of **a** energy absorber, **b** diaphragm used in the validation study

as the area under the load-displacement curve or calculated using the following equation;

$$EA = \int_0^{\delta_c} P\, d\delta \tag{2}$$

where δ_c refers the maximum amount displacement of the crash absorber, and P represents the crash force. In this study, δ_c is taken as 200 mm.

SEA refers to the ratio of total energy absorbed (EA) to the mass of the crash absorber structure (m) such that

$$SEA = \frac{EA}{m} \tag{3}$$

3 Finite element modeling

The finite element (FE) model is created in accordance with the definitions set out in Xu et al. (2019a), and solved using explicit finite element package LS-DYNA. The energy absorber structure and the diaphragms are constructed with the dimensions shown in Fig. 2a and b, respectively.

The FE model of the energy absorber structure and the impactor are shown in Fig. 3. The bottom plate is fixed, while the other plate (impactor) moves only on the impact axis. A solid box is created to be used as an impactor. The impactor also moves only on the impact axis at a steady speed of 2000 mm/s. The impactor is modeled with hexahedral solid elements with constant stress solid element formulation. Quadrilateral shell elements are used to model the rest of the structure, where Belytschko–Tsay shell element formulation with two integration points through the thickness are used as described in Xu et al. (2019a).

Figure 3 shows the detailed FE model used in validation study. In this model, outer tube walls are divided into sub-surfaces with lines between the edges of the diaphragms. Diaphragms are also divided into sub-surfaces with offset curves from the diaphragm edges. Thus, a better mesh

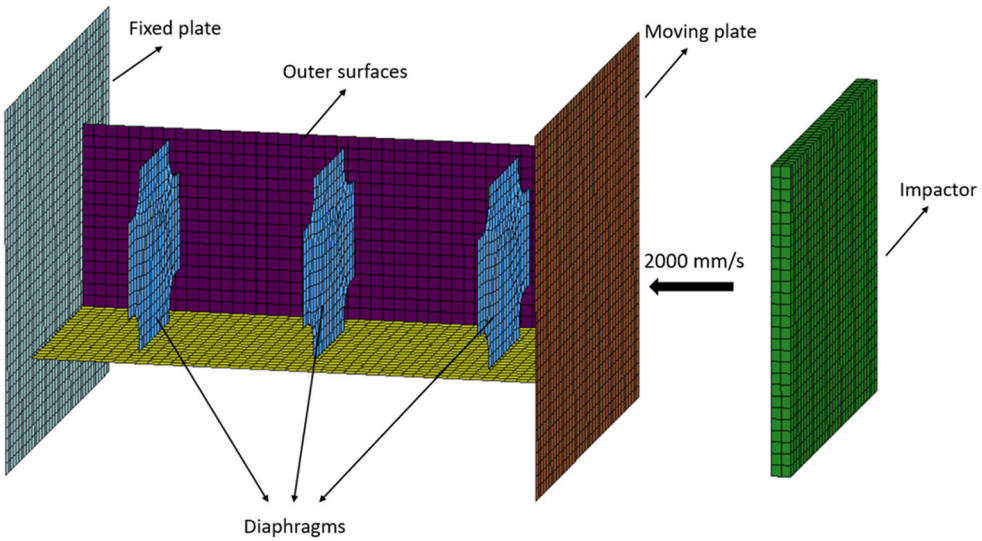

Fig. 3 Finite element model used in the validation study

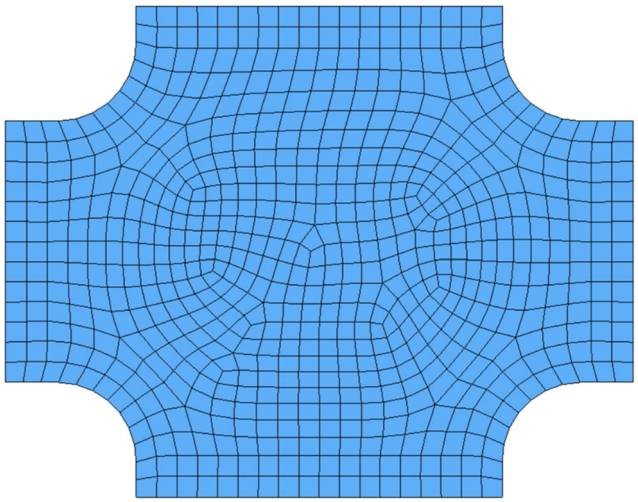

Fig. 4 Diaphragm mesh model used in validation study

structure is created in the regions diaphragms contact the outer tube walls (see Fig. 4).

A mesh converge study is performed to determine the suitable element size to model the energy absorber structure and plates on both sides (see Fig. 5). It is found that 5 mm element size is sufficient to model this energy absorber structure and plates on both sides. Note also that 10 mm element size is chosen for the rigid impactor.

In the FE model, two types of contact algorithms are used. "AUTOMATIC_ SURFACE_TO_SURFACE" is used to define the contact between the impactor and the top plate. "AUTOMATIC_SINGLE_SURFACE" is used to define the contact between the outer walls of the energy absorber, diaphragms and plates on both sides. Static and dynamic friction coefficients are defined as 0.3 and 0.2, respectively, for all contact algorithms as described in Xu et al. (2019a).

Table 1 Material properties for MAT24 model defined in Xu et al. (2019a)

Mechanical parameters	Values
Density (kg/mm^3)	7.85×10^{-6}
Young's modulus (GPa)	206
Poisson's ratio	0.3
Yield stress (MPa)	335

Note that the diaphragms are connected to the tube by welding. To model this connection, the diaphragms are connected to the tube by mesh connectivity in the FE model. Therefore, no contact definition is needed to capture this connection in the FE model.

Outer walls, diaphragms and plates on both sides are modeled using the MAT24-PIECEWISE_LINEAR_PLASTICITY material model and impactor is modeled using the MAT20-RIGID material model in the LS-DYNA software as described in Xu et al. (2019a). The material parameters given in Table 1 and true stress – true plastic strain values given in Table 2 are taken from Xu et al. (2019a), where quasi-static tensile tests are conducted to obtain material behavior.

4 Validation of the finite element model

In the validation analysis, the energy absorber structure for which experimental results are available is used. Xu et al. (2019a) compared the results of their finite element model with the results of their experiments, which were carried out with a hydraulic press with a compression velocity of 1200 mm/s for a total displacement of 200 mm. They found that their finite element model had adequate accuracy. In the

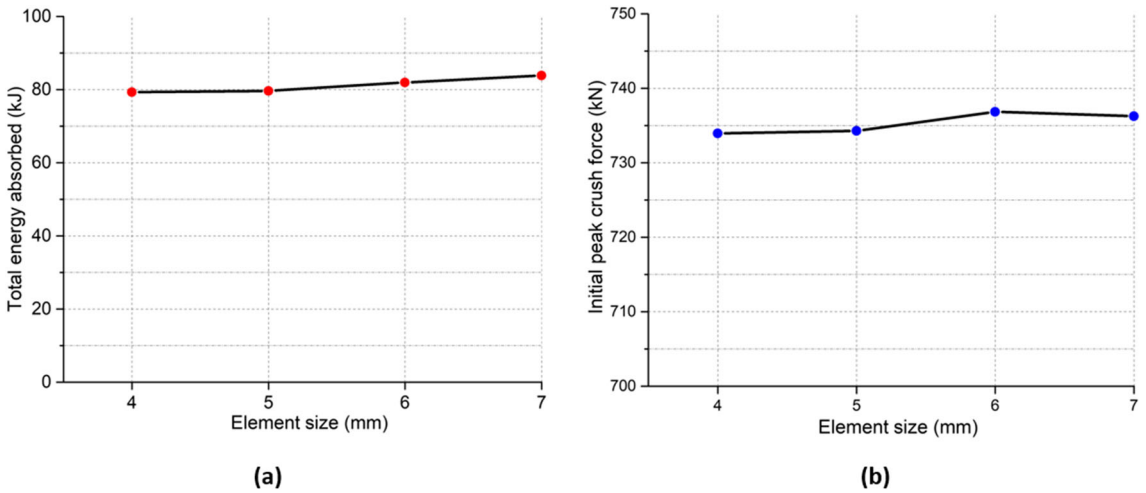

Fig. 5 Results of the mesh convergence analysis for energy absorber structure and plates at both sides for **a** total energy absorbed, **b** initial peak crash force

Table 2 True stress–true plastic strain values used in the FE model

σ_t (MPa)	335	408	476	584	695	772	849	1602
ε_p	0	0.005	0.018	0.066	0.133	0.170	0.253	0.794

experiments, the wall thicknesses as well as the diaphragm thickness are all taken as 4 mm (that is, $A = B = C_u = 4$ mm is used). In this paper, this crash absorber configuration of Xu et al. (2019a) is considered the baseline design.

We validate our finite element model by comparing with the numerical and experimental results given in Xu et al. (2019a). Table 3 shows that the EA and IPCF results of our finite element model are in good agreement with the experimental and numerical results obtained by Xu et al. (2019a). The error in EA prediction is found to be 1.5%, whereas the error in IPCF prediction is observed to be 4.2%. These errors are considered to be appropriate for a nonlinear phenomenon like crash.

Figures 6 and 7 provide graphical comparison of the FE results of this study to the experimental and FE results of Xu et al. (2019a). Figure 6 indicates that the peaks in the force-displacement curve obtained by using our FE model are similar to those of the experimental and numerical results of Xu et al. (2019a). The explanation for the disparity in experimental and numerical curves after a displacement of 150 mm is due to the tearing of the welds used in the development of the experimental model, as explained in Xu et al. (2019a).

Figure 7 demonstrates the comparison of lobe formation in our FE model to those of the numerical and experimental results given in Xu et al. (2019a). Lobe formations are observed to be similar in all three models at the same displacement values, which shows that our FE model is accurate enough to conduct further analysis on the optimization of the crash absorber.

5 Options to improve crashworthiness performance

A surrogate-based optimization study is conducted, where the wall thicknesses of the absorber and the diaphragms, the locations of the diaphragms, and the taper angle are taken as design variables to optimize the crashworthiness performance of the absorber. The effect of each design option on crashworthiness performance is evaluated by solving a series of design optimization problems, and compared with the baseline design discussed in Section 4. A successive approach is used in this study, where the optimum design variables obtained from a previous optimization problem is used as the initial design of the following optimization problem. Brief explanations of the surrogate models used in this study are given in Appendix 1. Accuracies of the surrogate models are evaluated at some randomly chosen test points, and the errors in the constructed surrogate models are presented in Appendix 2. Optimization results obtained through each surrogate model are given in Appendix 3. The surrogate model generation and optimization are both conducted by using MATLAB in this study. The optimization problems are solved by using *fmincon* function of MATLAB based on the sequential quadratic programming algorithm. To increase the probability of finding the global minimum, a multi-start approach is used.

Note that all design variables could have been combined in one optimization formula instead of adopting the successive approach. However, this practice would increase the number of training points to very large values. For instance, the number of coefficients in a fourth order polynomial in terms of seven design variables is 330, so we would need around five hundred training points. Therefore, a successive approach is preferred to alleviate the computational cost.

5.1 Optimization of the tube and the diaphragm thicknesses

First, the tube and the diaphragm thicknesses are optimized, where all diaphragm thicknesses are taken to be the same. That is, the thicknesses of diaphragms C, D and E are all taken to be equal to C_u (see Fig. 3). In this subsection,

Table 3 Comparison of the FE result of this study to the experimental and FE results of Xu et al. (2019a), where deformation distance is 200 mm

	IPCF (kN)	Error (%)	EA (kJ)	Error (%)
Experimental result of Xu et al. (2019a)	702.8	-	78.15	-
FE result of Xu et al. (2019a)	697.9	0.7%	75.80	3.0%
FE result of the present study	734.0	4.2%	79.31	1.5%

*SEA = 17.49 kJ/kg for the FE result of the present study

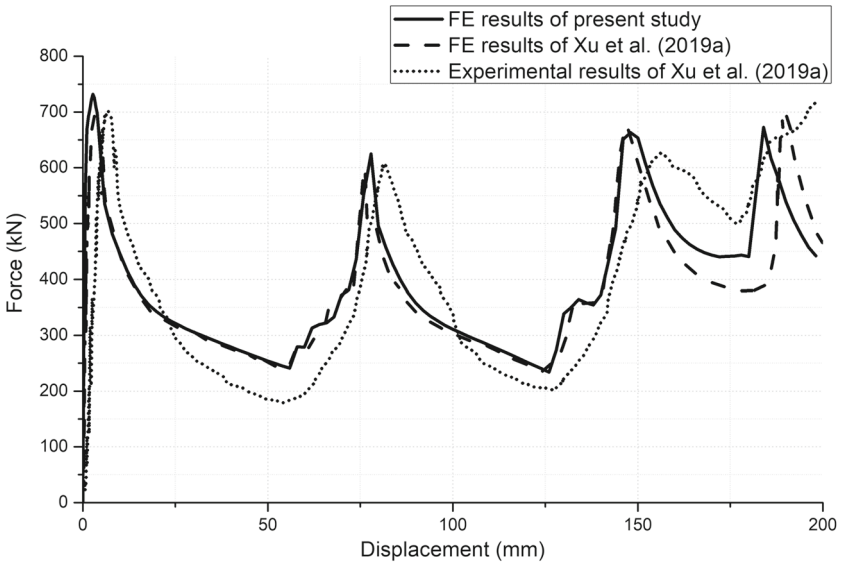

Fig. 6 Comparison of the force-displacement result of this study to the experimental and FE results of Xu et al. (2019a)

the other design options (i.e., diaphragm placement and taper angle) are not taken into account. The optimization problems for maximum SEA stated in (1) is solved.

A surrogate-based approach is used in optimization. Surrogate models are constructed by using 57 training points, where 30 points are generated by using Latin hypercube sampling and 27 points (corresponding to three variables and three levels) are generated using full fractional design. This is inspired from one of the papers by Prof. Haftka where FCCCD and LHS were combined to generate training points in surrogate model construction (Qu et al. 2003). The reason for this practice was that they found that LHS might fail to sample points near some corners of the design space, leading to poor accuracy around these corners. Following this reasoning, we combined FFD and LHS to generate training points in this study.

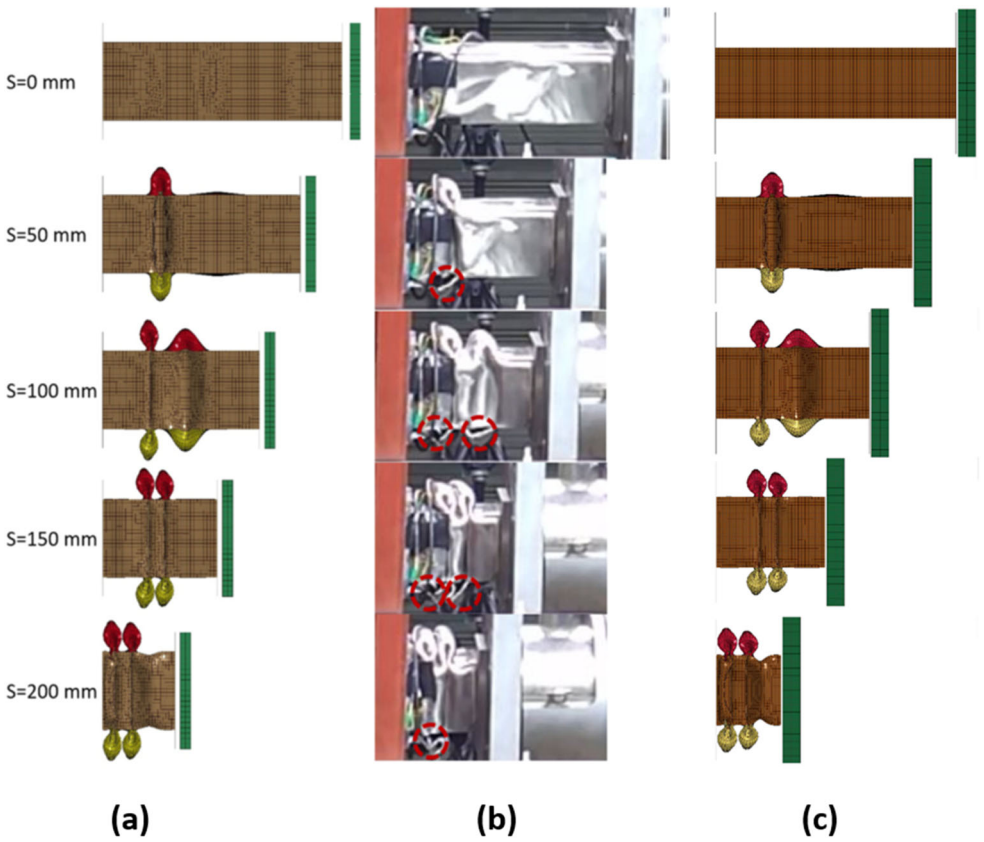

Fig. 7 Visual comparison of the force-displacement result of this study to the (**a**) FE results of Xu et al. (2019a), **b** experimental results of Xu et al. (2019a), **c** FE results of present study

Table 4 Results of optimization of the tube and diaphragm thicknesses

Design variables	A (mm)	6.00
	B (mm)	6.00
	C_u (mm)	2.95
Results	SEA prediction (kJ/kg)	27.44
	SEA FEA result (kJ/kg)	27.85
	SEA error (%)	1.5%
	EA prediction (kJ)	169.4
	EA FEA result (kJ)	170.8
	EA error (%)	0.8%
	SEA improvement (%)	59.2%

Table 4 shows that SEA can be increased by 59.2% compared to those of the baseline model. Notice that the SEA value of the baseline model is 17.49 kJ/kg, and the SEA value of the optimized design is 27.85 kJ/kg. The wall thicknesses A and B take their upper limit values of 6 mm, which is larger than that of the baseline model. The upper limit values of A and B are taken from the reference study, Xu et al. (2019b). As the optimum values of A and B take their upper limits, there is more room for improvement in SEA. However, this will increase the mass of the crash absorber, and this practice might not be preferred. The optimum value of the diaphragm thicknesses C_u is found to be 2.95 mm, which is smaller than that of the baseline design. The comparison of the force-displacement results of the baseline design and the optimum design based on thickness optimization is shown in Fig. 8.

5.2 Diaphragm location optimization

Next, diaphragm locations are optimized for maximum SEA. The locations of diaphragms C, D and E are varied by moving them closer to or away from the impact (see Fig. 9). Three design variables are used in this study: (i) location of the diaphragm closest to impact (L_C), (ii) location of the diaphragm in the middle of the crash absorber (L_D), (iii) location of the diaphragm furthest to the impact (L_E).

The optimization values of the outer tube edge thicknesses (A and B) and diaphragm thickness (C_u) are used. The optimization problem for diaphragm location optimization study can be stated as

$$\begin{aligned}
\text{Find} \quad & L_C, L_D, L_E \\
\text{Max} \quad & \text{SEA}(L_C, L_D, L_E) \\
\text{s.t.} \quad & \text{EA}(L_C, L_D, L_E) \geq 70 \text{ kJ} \\
& -30 \text{ mm} \leq L_C \leq 30 \text{ mm} \\
& -30 \text{ mm} \leq L_D \leq 30 \text{ mm} \\
& -30 \text{ mm} \leq L_E \leq 30 \text{ mm} \\
& A = 6.00 \text{ mm} \\
& B = 6.00 \text{ mm} \\
& C_u = 2.95 \text{ mm}
\end{aligned} \tag{4}$$

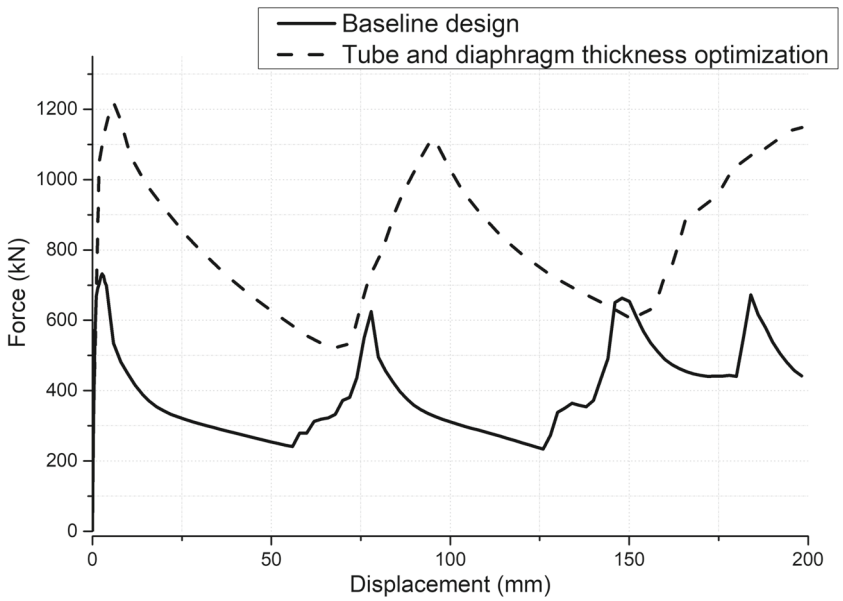

Fig. 8 Comparison of the force-displacement results of the baseline design and the optimum design based on thickness optimization

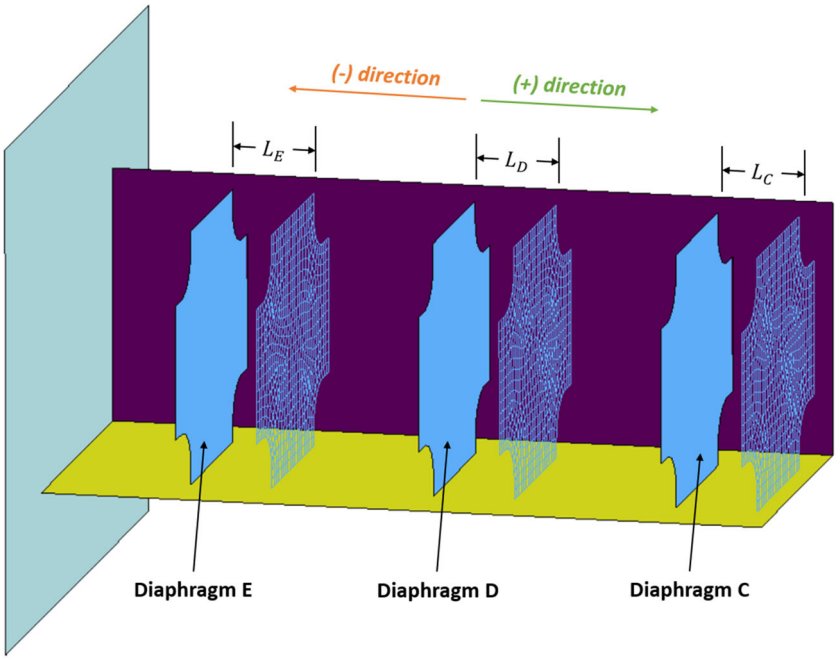

Fig. 9 Locations of the diaphragms C, D and E

The training points are generated in the same manner as described in Section 5.1. Table 5 shows the optimization results. Diaphragm location optimization leads to a SEA improvement from 59.2 to 66.9% (additional 7.7% improvement compared to the thickness optimization).

Table 5 shows that SEA can be improved by moving the diaphragms closer to the impact side. The location values L_D and L_E take their upper limit values. The upper limits of L_D and L_E are taken based on intuition, and the spacing between the diaphragms. These upper limits values can be changed, and investigation of the effects of these changes is left for a future study. It is observed that increasing the distance between L_E and the bottom plate leads to a more efficient local deformation in that region and thereby results in a higher SEA values. It is also found that the diaphragm closest to the impact is also moved further to the impact side, but not as much as the other two diaphragms. The comparison of the force-displacement results of the baseline design and the optimum design based on diaphragm location optimization is shown in Fig. 10.

5.3 Taper angle optimization

Next, a taper angle is applied to all outer edges of the rectangular tube (see Fig. 11). The optimization thickness and location values obtained in earlier subsections are used. The optimization study can be stated as

$$\begin{array}{ll} \text{Find} & \alpha \\ \text{Max} & \text{SEA}(\alpha) \\ \text{s.t.} & \text{EA}(\alpha) \geq 70 \text{ kJ} \\ & 0^\circ \leq \alpha \leq 10^\circ \\ & A = 6.00 \text{ mm} \\ & B = 6.00 \text{ mm} \\ & C_u = 2.95 \text{ mm} \\ & L_C = 2.67 \text{ mm} \\ & L_D = 30.00 \text{ mm} \\ & L_E = 30.00 \text{ mm} \end{array} \tag{5}$$

In surrogate-based optimization, 11 design points created by dividing the taper angle range (0 to 10°) into 1°

Table 5 Results of diaphragm location optimization

Design variables	L_C (mm)	+2.67
	L_D (mm)	+30.00
	L_E (mm)	+30.00
Results	SEA prediction (kJ/kg)	28.26
	SEA FEA result (kJ/kg)	29.21
	SEA error (%)	3.3%
	EA prediction (kJ)	173.3
	EA FEA result (kJ)	179.1
	EA error (%)	3.4%
	SEA improvement (%)	66.9%

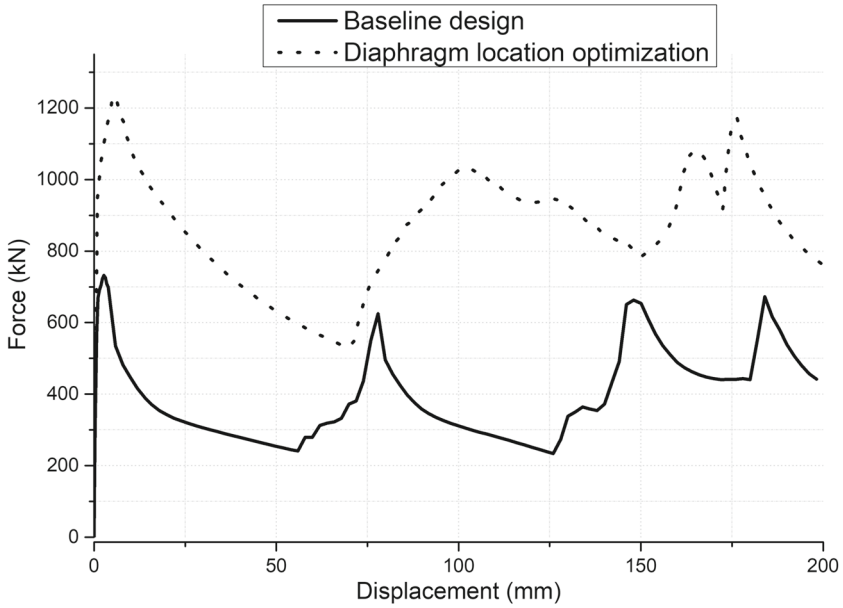

Fig. 10 Comparison of the force-displacement results of the baseline design and the optimum design based on diaphragm location optimization

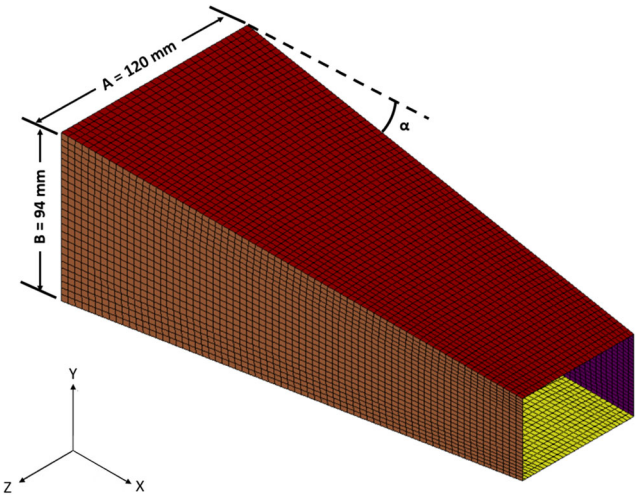

Fig. 11 Taper angle of the energy absorber

Table 6 Results of taper angle optimization

Design variable	α (°)	2.77
Results	SEA prediction (kJ/kg)	29.75
	SEA FEA result (kJ/kg)	29.64
	SEA error (%)	0.4%
	EA prediction (kJ)	169.8
	EA FEA result (kJ)	169.2
	EA error (%)	0.4%
	SEA improvement (%)	69.4%

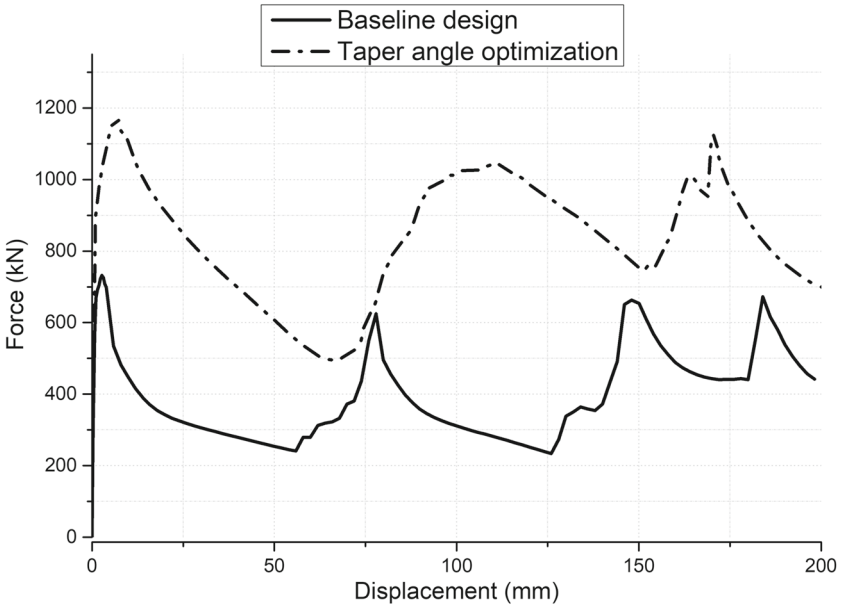

Fig. 12 Comparison of the force-displacement results of the baseline design and the optimum design based on taper angle optimization

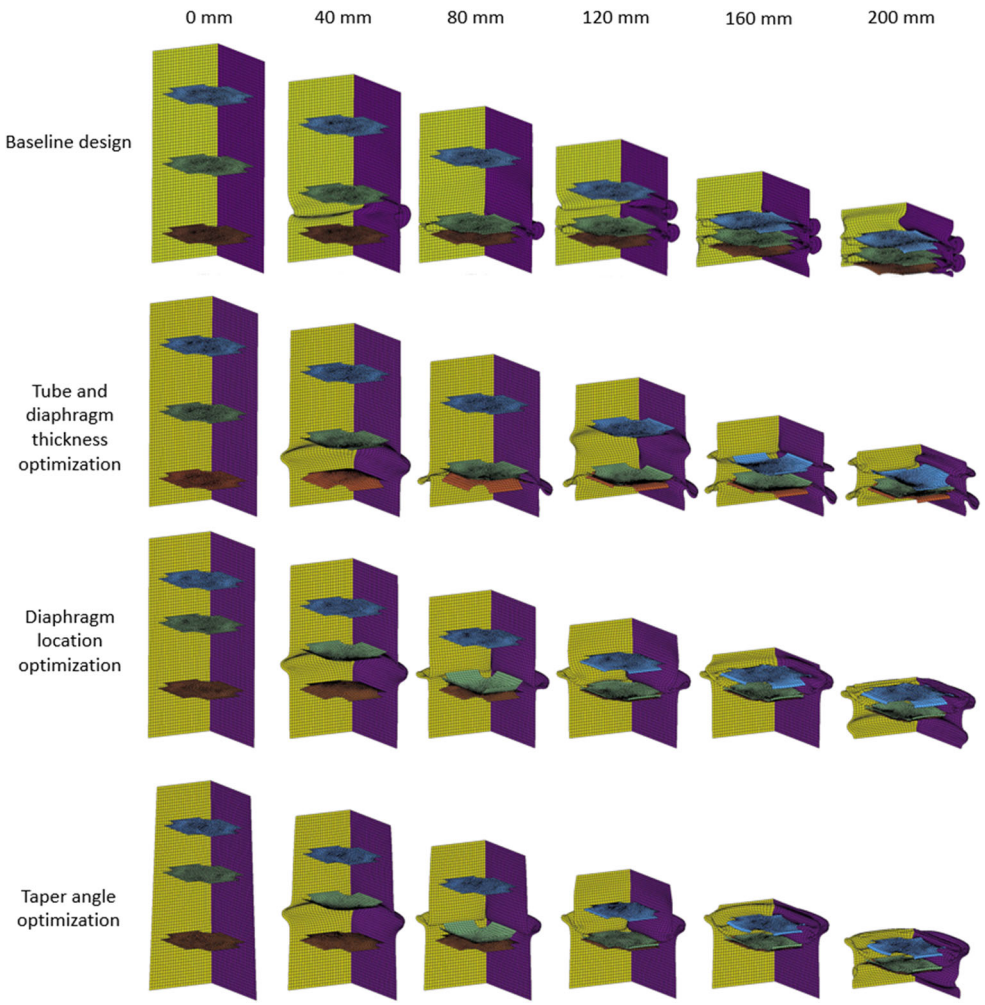

Fig. 13 Comparison of the deformation behavior of the baseline design, and successive optimum designs achieved through thickness, diaphragm location and taper angle optimization at various displacements of the impactor

intervals, starting from 0°. Table 6 shows that taper angle optimization increased the SEA improvement from 66.9 to 69.4% (additional 2.5% improvement compared to the diaphragm location optimization). It is found that the optimum value of the taper angle is 2.77° for this crash absorber. The comparison of the force-displacement results of the baseline design and the optimum design based on taper angle optimization is shown in Fig. 12.

Finally, the comparison of the deformation behavior of the baseline design, and successive optimum designs achieved through thickness, diaphragm location and taper angle optimization is shown in Fig. 13. It is seen that the deformation behavior of the crash absorber improves as the successive optimization progresses. It is also found that the baseline design collapses in symmetric mode whereas all other optimized designs collapse in extensional mode. Abramowicz and Jones (1986) showed that the extensional mode controls the static progressive buckling of square tubes (without diaphragms) when $w/t \leq 7.5$. We argue that the diaphragms might increase the threshold value of 7.5 to larger values. Therefore, the diaphragms improve the crash performance of the absorbers by activating the extensional collapse mode for larger values of w/t compared to crash absorbers without diaphragms.

6 Concluding remarks

In this study, a series of optimization studies was conducted on a rail vehicle crash absorber with diaphragms. Effects of changing tube edge and diaphragm thicknesses, diaphragm locations and taper angle were studied in an iterative fashion by subsequently solving the mentioned sub-problems. From the results of this study, the following conclusions were drawn:

- The diaphragms improved the crash performance of the absorbers by activating the extensional collapse mode for larger values of w/t compared to crash absorbers without diaphragms.
- Optimal tube and diaphragm dimensioning resulted in 59.2% increase in SEA compared to the baseline design. The tube wall thicknesses took their upper limit values, whereas the optimum value of the diaphragm thicknesses C_u was found to be smaller than that of the baseline design.
- Optimum diaphragm placement resulted in 7.7% more increase in SEA. This improvement was obtained by moving the diaphragms closer to the impact side. It was observed that increasing the distance between the diaphragm at the end and the bottom plate lead to a more efficient local deformation in that region and thereby resulted in a higher SEA values. It was also found that the diaphragm closest to the impact is also moved further to the impact side, but not as much as the other two diaphragms.
- Tapering resulted in an additional 2.5% SEA improvement. It was found that the optimum value of the taper angle is 2.77° for this crash absorber.
- It was observed that the largest effect on the optimum SEA response was provided by the optimization of the tube and the diaphragm thicknesses, followed by the optimization of the location of the diaphragms, and the tapering of the crash absorber.
- The successive iterative optimization approach is used in this study provided an overall 69.4% increase of the SEA value compared to that of the baseline design.
- The EA constraint in (1), (4) and (5) is intended to penalize designs that might maximize SEA but not provide enough EA (less than 70 kJ, required in this study). In this study, we found that the constraint did not become active in any of the optimization cases.

Lastly, some limitations of the current study can be listed as follows:

- Note that all design variables could have been combined in one optimization formula instead of adopting the successive approach. However, this practice would increase the number of training points to very large values. Therefore, a successive approach is preferred to alleviate the computational cost.
- It should be noted that the successive iterative optimization approach used in this paper may result in a final solution that is not necessarily the global optimum, because in each subsequent stage, the optimization searches within a sub-space of the overall design space. Also, the order of sequential sub-problems might influence the final solution.
- In optimization problems, some design variables reach their limits, and investigation of the effect of changing these limits is left for a future study.
- In this study, the peak force values were not penalized in optimization. It should be noted that a high peak force relates to high accelerations, which should be avoided in a crashworthy design. Also, crush force efficiency could be added as another objective in optimization. These exercises are subject of a future study.
- In this study, polynomial response surfaces and radial basis functions are used as surrogate models. The other types of surrogate models such as neural networks, Kriging, support vector regression, etc. could also be used.

Acknowledgements This paper is written for recognition of the Prof. Raphael (Rafi) T. Haftka's novel contributions in the field of structural and multidisciplinary design optimization. Rafi was a pioneer in our optimization community who rigorously contributed to the areas

of surrogate-based optimization, structural and multidisciplinary optimization, sensitivity analysis, reliability-based design optimization, optimization of laminated composite materials and others. The corresponding author is one of the PhD students of Rafi, and thankful to have had the privilege of collaborating, knowing and being friend to him.

Declarations

Conflict of interest The authors declare that they have no conflict of interest.

Replication of results The results provided in this paper are replicable. Interested readers can connect the corresponding author to get the training and test data used in construction of surrogate models.

Appendix 1. Brief explanations of the surrogate models used

In this study, response surface approximations and radial basis functions are used as surrogate models. Using response surface models, the response is approximated as:

$$\hat{f}(x) = b_0 + \sum_{i=1}^{L} b_i x_i + \sum_{i=1}^{L} b_{ii} {x_i}^2 + \sum_{i=1}^{L-1} \sum_{j=i+1}^{L} b_{ij} x_i x_{ij} + \ldots \tag{A1.1}$$

where $\hat{f}(x)$ refers to the prediction of response, L refers to the number of input variables, b_i, b_{ii} and b_{ij} refers to the parameters of response surface model obtained with regression (Myers et al. 2016). Quadratic, cubic and quartic response surface models are used in this study.

Using radial basis functions, the response is approximated as;

$$\hat{f}(x) = \sum_{i=1}^{n} \lambda_i \phi(\|x - x_i\|) \tag{A1.2}$$

where $\hat{f}(x)$ refers to the prediction of response, λ_i refers to parameters of radial basis functions, n refers to the number of training points, and $\phi(\|x - x_i\|)$ refers to the radial basis functions created with $\|x - x_i\|$ Euclidean norm, representing the radial distance r. The Euclidean norm is approximated as;

$$\|x - x_i\| = \sqrt{(x - x_i)^T (x - x_i)} \tag{A1.3}$$

In this equation, x represents the sampling point an x_i refers to the center [(Buhmann 2003)].

Thin-plate spline (A1.4), gaussian (A1.5) and multiquadric (A1.6) radial basis functions are used in this study. Formulations of these functions are shown below;

$$\phi(r) = r^2 \log(cr^2) \tag{A1.4}$$

$$\phi(r) = e^{-cr^2}, c > 0 \tag{A1.5}$$

$$\phi(r) = \sqrt{r^2 + c^2} \tag{A1.6}$$

The choice of parameter $c = 1$ is found suitable for most function appropriations (Wang et al. 2006). Note that the hyperparameter c could have been selected in such a way to minimize the generalized cross validation error (Rippa 1999).

Appendix 2. Errors in surrogate models

Accuracies of the surrogate models are computed by evaluating the performance of the surrogate models at test points. Every surrogate model is evaluated with 20 test points, created using Latin hypercube sampling. Normalized mean absolute error (n_{MAE}), normalized maximum absolute error (n_{MaxAE}) and normalized root mean square error (n_{RMSE}) error metrics are used to evaluate the performances of the surrogate models. Formulations of these error metrics are given below:

$$n_{MAE} = \frac{\sum_{i=1}^{n} \left|\hat{y}_i - y_i\right|}{n \times (y_{max} - y_{min})} \tag{A2.1}$$

$$n_{MaxAE} = Max\left(\frac{\left|\hat{y}_i - y_i\right|}{y_{max} - y_{min}}\right) \tag{A2.2}$$

$$n_{RMSE} = \frac{1}{y_{max} - y_{min}} \sqrt{\sum_{i=1}^{n} \frac{(\hat{y}_i - y_i)^2}{n}} \tag{A2.3}$$

In the formulas above, n refers to the number of test points. For test point i, $\hat{y}_i$ refers to the approximate result obtained from the surrogate model and y_i refers to the result of finite element analysis. Moreover, y_{max} and y_{min} represents the maximum and minimum results obtained from the finite element analyses in all test points.

The error metrics computed for all surrogate models constructed for this study are presented in Tables 7–9. Table 7 shows the error metrics of all surrogate models used in optimization of the tube and diaphragm thicknesses (in Section 5.1). Table 8 shows the error metrics of all surrogate models used in diaphragm location optimization (in Section 5.2). It is observed that all surrogate models have adequate accuracies. Table 9 shows the error metrics of all surrogate models used in taper angle optimization (in Section 5.3). It is observed that all surrogate models have adequate accuracies.

Table 7 Error metrics for all surrogate models used in tube and diaphragm thickness optimization (in Section 5.1)

Response	Metric	Quadratic RSM	Cubic RSM	Quartic RSM	Thin-plate spline RBF	Gaussian RBF	Multiquadric RBF
EA	n_{MAE}	0.05	0.04	0.03	0.03	0.08	0.03
	n_{MaxAE}	0.10	0.09	0.14	0.09	0.26	0.09
	n_{RMSE}	0.05	0.05	0.05	0.04	0.10	0.04
SEA	n_{MAE}	0.08	0.07	0.06	0.05	0.13	0.05
	n_{MaxAE}	0.20	0.17	0.25	0.16	0.35	0.15
	n_{RMSE}	0.10	0.09	0.09	0.07	0.16	0.07

Table 8 Error metrics for all surrogate models used in diaphragm location optimization (in Section 5.2)

Response	Metric	Quadratic RSM	Cubic RSM	Quartic RSM	Thin-plate spline RBF	Gaussian RBF	Multiquadric RBF
EA	n_{MAE}	0.20	0.20	0.22	0.17	0.15	0.15
	n_{MaxAE}	0.71	0.60	0.77	0.63	0.65	0.53
	n_{RMSE}	0.25	0.24	0.29	0.23	0.24	0.20
SEA	n_{MAE}	0.20	0.20	0.22	0.17	0.15	0.15
	n_{MaxAE}	0.71	0.60	0.77	0.63	0.65	0.53
	n_{RMSE}	0.25	0.24	0.29	0.23	0.24	0.20

Table 9 Error metrics for all surrogate models used in taper angle optimization for maximum SEA objective function (in Section 5.3)

Response	Metric	Quadratic RSM	Cubic RSM	Quartic RSM	Thin-plate spline RBF	Gaussian RBF	Multiquadric RBF
EA	n_{MAE}	0.06	0.05	0.04	0.02	0.06	0.02
	n_{MaxAE}	0.28	0.22	0.23	0.15	0.33	0.14
	n_{RMSE}	0.08	0.07	0.06	0.05	0.10	0.04
SEA	n_{MAE}	0.14	0.11	0.10	0.06	0.15	0.05
	n_{MaxAE}	0.68	0.54	0.55	0.35	0.70	0.34
	n_{RMSE}	0.21	0.16	0.15	0.11	0.22	0.11

Appendix 3. Optimization results obtained through each surrogate model

Table 10 shows the optimum designs for tube and diaphragm thickness optimization study. It is observed that the maximum SEA is obtained by using cubic response surface model. Table 11 shows the optimum designs for diaphragm location optimization study. Again, it is seen that the maximum SEA is obtained by using cubic response surface model. Table 12 shows the optimum designs for taper angle optimization study. This time, it is seen that the maximum SEA is obtained by using multiquadric radial basis function.

Table 10 Optimization results obtained through each surrogate model when tube and diaphragm thicknesses are optimized (in Section 5.1)

Surrogate model	A (mm)	B (mm)	C_u (mm)	SEA pred. (kJ/kg)	SEA FEA result (kJ/kg)	SEA error (%)	EA pred. (kJ)	EA FEA result (kJ)	EA error (%)
Thin-plate spline RBF	6.00	6.00	3.00	27.58	27.66	0.3	170.8	169.9	0.5
Gaussian RBF	5.86	5.94	2.41	28.75	27.39	4.8	175.4	162.1	7.6
Multiquadric RBF	6.00	6.00	2.97	27.57	27.73	0.6	170.6	170.2	0.2
Quadratic RSM	6.00	6.00	3.52	26.45	26.74	1.1	167.0	167.3	0.2
Cubic RSM	6.00	6.00	2.95	27.44	27.85	1.5	169.4	170.8	0.8
Quartic RSM	6.00	5.57	2.58	28.09	26.21	6.7	165.6	154.1	7.0

Table 11 Optimization results obtained through each surrogate model when diaphragm locations are optimized (in Section 5.2)

Surrogate model	A (mm)	B (mm)	C_u (mm)	SEA pred. (kJ/kg)	SEA FEA result (kJ/kg)	SEA error (%)	EA pred. (kJ)	EA FEA result (kJ)	EA error (%)
Thin-plate spline RBF	+0.61	+29.43	+30.00	28.63	28.73	0.3	175.6	176.2	0.3
Gaussian RBF	0.00	0.00	0.00	27.85	27.85	0.0	170.8	170.8	0.0
Multiquadric RBF	+0.15	+30.00	+30.00	28.63	28.65	0.1	175.6	175.7	0.1
Quadratic RSM	+4.49	+30.00	+27.55	27.04	28.05	3.8	165.8	172.0	3.8
Cubic RSM	+2.67	+30.00	+30.00	28.26	29.21	3.3	173.3	179.1	3.4
Quartic RSM	−7.94	−18.58	+0.39	27.62	26.96	2.4	169.4	165.3	2.4

Table 12 Optimization results obtained through each surrogate model when taper angle is optimized (in Section 5.3)

Surrogate model	α (°)	SEA pred. (kJ/kg)	SEA FEA result (kJ/kg)	SEA error (%)	EA pred. (kJ)	EA FEA result (kJ)	EA error (%)
Thin-plate spline RBF	2.78	29.74	29.62	0.4	169.7	169.0	0.4
Gaussian RBF	9.65	30.84	28.80	6.6	144.0	134.9	6.3
Multiquadric RBF	2.77	29.75	29.64	0.4	169.8	169.2	0.4
Quadratic RSM	0.00	29.91	29.21	2.3	182.8	179.1	2.0
Cubic RSM	0.89	29.45	29.32	0.4	176.4	175.8	0.4
Quartic RSM	1.22	29.72	29.25	1.6	176.5	173.8	1.5

References

Abolfathi M, Alavi Nia A (2018) Optimization of energy absorption properties of thin-walled tubes with combined deformation of folding and circumferential expansion under axial load. Thin-Walled Struct 130:57–70. https://doi.org/10.1016/j.tws.2018.05.011

Abramowicz W, Jones N (1986) Dynamic progressive buckling of circular and square tubes. Int J Impact Eng 4(4):243–270

Acar E, Guler MA, Gerçeker B, Cerit ME, Bayram B (2011) Multi-objective crashworthiness optimization of tapered thin-walled tubes with axisymmetric indentations. Thin-Walled Struct 49(1):94–105. https://doi.org/10.1016/j.tws.2010.08.010, http://www.sciencedirect.com/science/article/pii/S0263823110001400

Altin M, Acar E, Gůler MA (2018) Foam filling options for crashworthiness optimization of thin-walled multi-tubular circular columns. Thin-Walled Struct 131(131):309–323. https://doi.org/10.1016/j.tws.2018.06.043

Altin M, Kılınċkaya Ů, Acar E, Gůler MA (2019) Investigation of combined effects of cross section, taper angle and cell structure on crashworthiness of multi-cell thin-walled tubes. Int J Crashworth 2:121–136. https://doi.org/10.1080/13588265.2017.1410338

An X, Gao Y, Fang J, Sun G, Li Q (2015) Crashworthiness design for foam-filled thin-walled structures with functionally lateral graded thickness sheets. Thin-Walled Struct 91:63–71. https://doi.org/10.1016/j.tws.2015.01.011

Asanjarani A, Dibajian SH, Mahdian A (2017) Multi-objective crashworthiness optimization of tapered thin-walled square tubes with indentations. Thin-Walled Struct 116:26–36. https://doi.org/10.1016/j.tws.2017.03.015

Auersvaldt RR, Alves M (2015) Impact Behavior of Windowed Polygonal Tubes. Int J Adv Mech Aeronaut Eng 2(1):26–30, http://journals.theired.org/journals/paper/details/5478.html

Buhmann MD (2003) Radial basis functions: theory and implementations, vol 12. Cambridge University Press

Deng X, Liu W (2019) Experimental and numerical investigation of a novel sandwich sinusoidal lateral corrugated tubular structure under axial compression. Int J Mech Sci 151:274–287. https://doi.org/10.1016/j.ijmecsci.2018.11.010

Dong HP, Gao GJ, Xie SC, Li J (2015) Collision performance of bitubular tubes with diaphragms. J Cent South Univ 22(9):3657–3665. https://doi.org/10.1007/s11771-015-2907-x

Fang J, Sun G, Qiu N, Kim NH, Li Q (2017) On design optimization for structural crashworthiness and its state of the art. Struct Multidiscip Optim 55(3):1091–1119

Gao G, Wang S (2019) Crashworthiness of passenger rail vehicles: a review. Int J Crashworth 24(6):664–676. https://doi.org/10.1080/13588265.2018.1511233

Gao G, Dong H, Tian H (2014) Collision performance of square tubes with diaphragms. Thin-Walled Struct 80:167–177. https://doi.org/10.1016/j.tws.2014.03.007

Goel T, Haftka RT, Shyy W, Queipo NV (2007) Ensemble of surrogates. Struct Multidiscip Optim 33(3):199–216

Mamalis AG, Manolakos DE, Ioannidis MB, Kostazos PK, Hassiotis G (2001) Finite element simulation of the axial collapse of thin-wall square frusta. Int J Crashworth 6(2):155–164. https://doi.org/10.1533/cras.2001.0169

Ming S, Zhou C, Li T, Song Z, Wang B (2019) Energy absorption of thin-walled square tubes designed by kirigami approach. Int J Mech Sci 157-158(157-158):150–164. https://doi.org/10.1016/j.ijmecsci.2019.04.032

Myers RH, Montgomery DC, Anderson-Cook CM (2016) Response surface methodology: process and product optimization using designed experiments. Wiley

Nagel GM, Thambiratnam DP (2004) Dynamic simulation and energy absorption of tapered tubes under impact loading. Int J Crashworth 9(4):389–399. https://doi.org/10.1533/ijcr.2004.0298

Nikkhah H, Guo F, Chew Y, Bai J, Song J, Wang P (2017) The effect of different shapes of holes on the crushing characteristics of aluminum square windowed tubes under dynamic axial loading. Thin-Walled Struct 119:412–420. https://doi.org/10.1016/j.tws.2017.06.036

Nikkhah H, Baroutaji A, Olabi AG (2019) Crashworthiness design and optimisation of windowed tubes under axial impact loading. Thin-Walled Struct 142(142):132–148. https://doi.org/10.1016/j.tws.2019.04.052

Peng Y, Deng W, Xu P, Yao S (2015) Study on the collision performance of a composite energy-absorbing structure for subway vehicles. Thin-Walled Struct 94:663–672. https://doi.org/10.1016/j.tws.2015.05.016

Qi C, Yang S, Dong F (2012) Crushing analysis and multiobjective crashworthiness optimization of tapered square tubes under oblique impact loading. Thin-Walled Struct 59:103–119, https://doi.org/10.1016/j.tws.2012.05.008, http://www.sciencedirect.com/science/article/pii/S0263823112001474

Qu X, Haftka RT, Venkataraman S, Johnson TF (2003) Deterministic and reliability-based optimization of composite laminates for cryogenic environments. AIAA J 41(10):2029–2036

Queipo NV, Haftka RT, Shyy W, Goel T, Vaidyanathan R, Tucker PK (2005) Surrogate-based analysis and optimization. Progress Aerospace Sci 41(1):1–28

Rippa S (1999) An algorithm for selecting a good value for the parameter c in radial basis function interpolation. Adv Comput Math 11(2):193–210

Roux W, Stander N, Haftka RT (1998) Response surface approximations for structural optimization. Int J Numer Methods Eng 42(3):517–534

Song J (2013) Numerical simulation on windowed tubes subjected to oblique impact loading and a new method for the design of obliquely loaded tubes. Int J Impact Eng 54:192–205. https://doi.org/10.1016/j.ijimpeng.2012.11.005

Song J, Guo F (2013) A comparative study on the windowed and multicell square tubes under axial and oblique loading. Thin-Walled Struct 66:9–14. https://doi.org/10.1016/j.tws.2013.02.002

Song X, Sun G, Li G, Gao W, Li Q (2013) Crashworthiness optimization of foam-filled tapered thin-walled structure using multiple surrogate models. Struct Multidiscip Optim 47(2):221–231. https://doi.org/10.1007/s00158-012-0820-6

Tarlochan F, Samer F, Hamouda AM, Ramesh S, Khalid K (2013) Design of thin wall structures for energy absorption applications: Enhancement of crashworthiness due to axial and oblique impact forces. Thin-Walled Struct 71:7–17. https://doi.org/10.1016/j.tws.2013.04.003

Taştan A, Acar E, Gůler MA, Kılımathnčkaya U (2016) Optimum crashworthiness design of tapered thin-walled tubes with lateral circular cutouts. Thin-Walled Struct 107:543–553. https://doi.org/10.1016/j.tws.2016.07.018

Tyan M, Lee JW (2019) Efficient multi-response adaptive sampling algorithm for construction of variable-fidelity aerodynamic tables. Chin J Aeronaut 32(3):547–558. https://doi.org/10.1016/j.cja.2018.12.012

Wang CY, Li Y, Zhao WZ, Zou SC, Zhou G, Wang YL (2018) Structure design and multi-objective optimization of a novel crash box based on biomimetic structure. Int J Mech Sci 138-139:489–501. https://doi.org/10.1016/j.ijmecsci.2018.01.032

Wang L, Beeson D, Wiggs G, Rayasam M (2006) A comparison meta-modeling methods using practical industry requirements. In: 47Th AIAA/ASME/ASCE/AHS/ASC structures, structural dynamics, and materials conference 14th AIAA/ASME/AHS adaptive structures conference 7th, pp 1811

Wang Z, Li Z, Shi C, Zhou W (2019) Mechanical performance of vertex-based hierarchical vs square thin-walled multi-cell structure. Thin-Walled Struct 134:102–110. https://doi.org/10.1016/j.tws.2018.09.017

Wu S, Zheng G, Sun G, Liu Q, Li G, Li Q (2016) On design of multi-cell thin-wall structures for crashworthiness. Int J Impact Eng 88:102–117. https://doi.org/10.1016/j.ijimpeng.2015.09.003

Xiang J, Du J (2017) Energy absorption characteristics of bio-inspired honeycomb structure under axial impact loading. Materials Science and Engineering: A 696:283–289, https://doi.org/10.1016/j.msea.2017.04.044, http://www.sciencedirect.com/science/article/pii/S0921509317304951

Xiang J, Du J, Li D, Scarpa F (2017) Numerical analysis of the impact resistance in aluminum alloy bi-tubular thin-walled structures designs inspired by beetle elytra. J Mater Sci 52(22):13247–13260. https://doi.org/10.1007/s10853-017-1420-z

Xie S, Yang W, Li H, Wang N (2017) Impact characteristics and crashworthiness of multi-cell, square, thin-walled, structures under axial loads. Int J Crashworth 22(5):503–517. https://doi.org/10.1080/13588265.2017.1281081

Xu P, Xu K, Yao S, Yang C, Huang Q, Zhao H, Xing J (2019a) Parameter study and multi-objective optimisation of an axisymmetric rectangular tube with diaphragms for subways. Thin-Walled Struct 136:186–199. https://doi.org/10.1016/j.tws.2018.12.025

Xu P, Shang Y, Jiang S, Yao S, Xu K, Xing J, Zhao H, Chen Z (2020) Theoretical development and multi-objective optimisation of a double-tapered rectangular tube with diaphragms. https://doi.org/10.1080/13588265.2020.1785109

Xu X, Zhang Y, Chen X, Liu Z, Xu Y, Gao Y (2019b) Crushing behaviors of hierarchical sandwich-walled columns. Int J Mech Sci:161–162. https://doi.org/10.1016/j.ijmecsci.2019.105021

Yao S, Xiao X, Xu P, Qu Q, Che Q (2018) The impact performance of honeycomb-filled structures under eccentric loading for subway vehicles. Thin-Walled Struct 123:360–370. https://doi.org/10.1016/j.tws.2017.10.031

Zhang X, Zhang H (2016) Crush resistance of square tubes with various thickness configurations. Int J Mech Sci 107:58–68. https://doi.org/10.1016/j.ijmecsci.2016.01.003

Zhou H, Xu P, Xie S (2017) Composite energy-absorbing structures combining thin-walled metal and honeycomb structures. Proc Inst Mech Eng Part F: J Rail Rapid Transit 231(4):394–405. https://doi.org/10.1177/0954409716631579

Zou X, jun Gao G, peng Dong H, Li J, sai Zhou X, Chen W, yuan Guan W (2017a) Crushing analysis and multi-objective optimization of bitubular hexagonal columns with ribs. J Cent South Univ 24(5):1164–1173. https://doi.org/10.1007/s11771-017-3519-4

Zou X, Gao G, Dong H, Xie S, Chen G, Tan T (2017b) Crashworthiness analysis and structural optimisation of multi-cell square tubes under axial and oblique loads. Int J Crashworth 22(2):129–147. https://doi.org/10.1080/13588265.2016.1235109